Chapter 4

Synthesis and Spectroscopy of Ruthenium(II)/7-Deazaguanine-Modified DNA Assemblies[‡]

[‡]Synthesis of the ruthenium(II) intercalator performed by Dr. Matthias M. Manger

4.1 Introduction

Chapters 2 and 3 detailed photoinduced DNA-mediated charge transfer between the modified base 7-deazaguanine and the intercalator ethidium or the modified base 2-aminopurine. Systematic investigation of ethidium excited-state reactivity with 7-deazaguanine at a distance through the DNA π stack revealed a shallow distance dependence[1a] and ultrafast charge transfer rates that correlated to the motion of the intercalator within the base stack.[2] Similar ultrafast charge transfer rates were observed for intrastrand charge transfer between bases, specifically 2-aminopurine and guanine or 7-deazaguanine, in DNA.[3,4] Although mechanisms other than electron transfer may be systematically ruled out, charge transfer intermediates were difficult to observe. For this reason we sought to utilize other reactants that might allow for the identification of intermediates in the DNA-mediated charge transfer process. This chapter outlines the synthesis of DNA duplexes modified with 7-deazaguanine and a covalently tethered ruthenium(II) intercalator. Both steady-state and time-resolved spectroscopies will be presented to characterize the electron transfer reaction.

Transition metal complexes of the type $[Ru(L)_2dppz]^{2+}$, (L = 2,2'-bipyridine (bpy) and 1,10-phenanthroline (phen), dppz = dipyridophenazine, Figure 4.1)[5,6] are well-known DNA intercalators. In aqueous solutions, their luminescence is quenched by proton interactions with the nitrogens on the phenazine portion of the dppz ligand.[7,8] Upon intercalation of the dppz moiety into the DNA base stack, the phenazine nitrogens become protected from solvent, thus allowing the complexes to emit (λ_{max} ca. 610 nm) when excited in their metal-to-ligand charge transfer (MLCT) bands. This makes them ideal probes to study photoinduced charge transfer through DNA, since only those metal complexes bound to the double helix will be observed when examining the luminescence spectroscopy of the intercalator. Indeed, a number of studies have examined the charge transfer behavior of these molecules in the presence of DNA.[9–11]

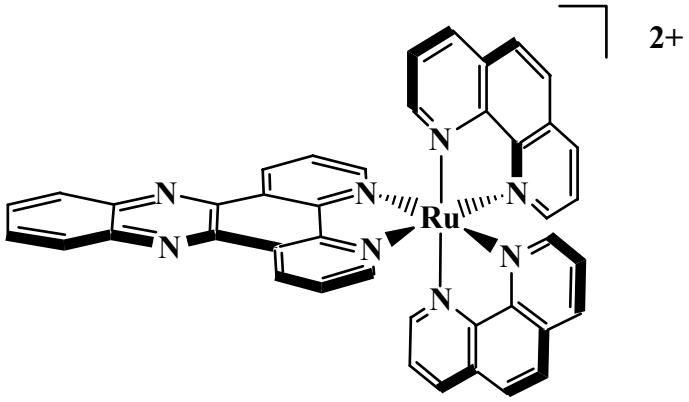

E(*2+/1+) = 1.5 V

Figure 4.1 Structure and excited-state potential of $[Ru(phen)_2dppz]^{2+}$.

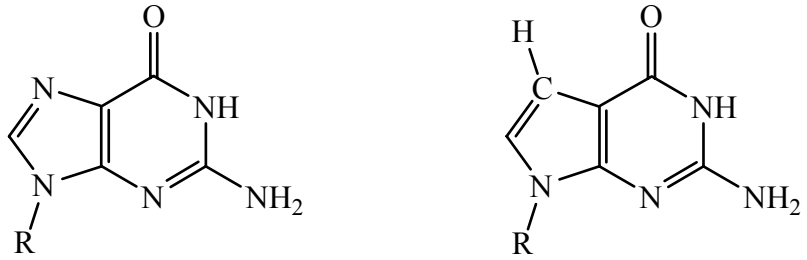

Guanine (G)
E_{ox}=1.3 V

Deazaguanine (Z)
E_{ox}=1.0 V

Figure 4.2 Structures and oxidation potentials of guanine (G) and deazaguanine (Z).[1]

As detailed in Chapters 2 and 3, 7-deazaguanine (Z) differs from guanine (G) solely in the change of a nitrogen to a C-H unit (Figure 4.2). Its hydrogen bonding, stacking, and structural stability in DNA double helices are very similar to that of the natural base guanine. Importantly, however, Z is 0.3 V easier to oxidize than G.[1] This property can be utilized to study the effect of driving force on DNA-mediated charge transfer or, alternatively, to examine systems where charge transfer does (Z) and does not (G) take place. Both methods have been utilized in our laboratory, and each has provided further evidence that charge transfer between well-coupled reactants through the DNA π stack is a fast and efficient process.

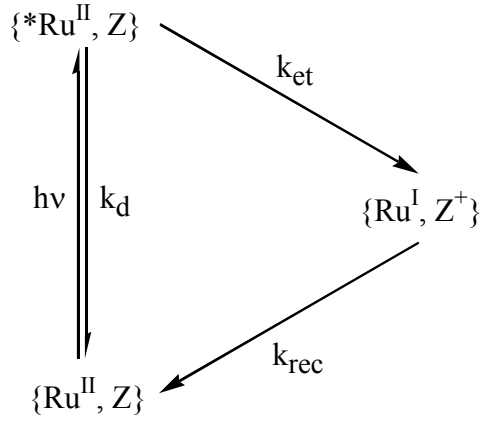

Figure 4.3 Proposed electron transfer cycle between $[Ru(phen)_2dppz]^{2+}$ (Ru) and 7-deazaguanine (Z).

Because of the unique spectroscopy of ruthenium(II) intercalators and the unique redox chemistry of 7-deazagaunine, we decided to study the photoinduced charge transfer reaction between Z and a ruthenium intercalator covalently tethered to the end of a DNA duplex. The overall scheme for the reaction is shown in Figure 4.3. The ruthenium intercalator is excited with visible light (λ_{exc} = 480 nm). The excited state may either decay back to the ground state (both radiatively and non-radiatively) or react with 7-deazaguanine to form a ruthenium(I) and 7-deazaguanine radical species. These may then participate in back electron transfer to bring the system back to its original state.

The driving force for charge transfer between *Ru(II) and Z is ca. ΔG = -0.5 V. Based on the potentials of the ruthenium excited state and guanine, *Ru(II) should be able to directly oxidize guanines in DNA as well (ΔG = -0.2 V). However, previous experiments from our laboratory have shown no evidence that this occurs.[12] In fact, the quantum yields of $[Ru(phen)_2dppz]^{2+}$ luminescence are higher in guanine containing DNA (poly d(GC)) than any other combination of sequences.[10] The explanation for this lies in the nature of the $[Ru(phen)_2dppz]^{2+}$ excited state. The excited state that initiates the reaction results from a metal-to-ligand charge transfer directed onto the dppz portion of the metal complex. When intercalated into DNA, the dppz is in intimate contact with

the π stack and would be the portion of the molecule accepting an electron from guanine. The extra electron density makes accepting an electron unfavorable when used with guanines in DNA. Using 7-deazaguanine, however, provides enough driving force to overcome this effect, and charge transfer behavior may be observed. These subtle yet unique properties allow us to study charge transfer through the DNA double helix in assemblies where photoinduced charge transfer occurs (Ru/Z) while using Ru/G assemblies as reference samples where no charge transfer takes place.

4.2 Experimental Section

Materials. Reagents for DNA oligonucleotide synthesis were obtained from Glen Research. QAE-A25 anion exchange resin was purchased from Aldrich. Unless otherwise noted, all other chemicals were purchased from Fluka or Aldrich and used without further purification. Dipyrido[3,2-a:2′,3′-c]phenazine (dppz),[13,14] $[Ru(phen)_2dppz]Cl_2$,[15,16] $[Ru(CO)_2(phen)Cl_2]$[17] and $[Ru(bpy)_2bpy']Cl_2$[12] (bpy'=4-butyric acid-8'-methyl bipyridyl) were prepared according to published procedures.

Instrumentation. NMR spectra were taken on a General Electric QE PLUS 300 MHz instrument or a Varian Inova-500 instrument using solvent as the internal standard. UV-visible spectra were measured on a Hewlett Packard HP8452A or a Beckmann DU 7400 UV-visible spectrophotometer. CD spectra were recorded on a JASCO J-600 spectropolarimeter. Steady-state emission from 500–800 nm was measured using an ISS K2 spectrofluorometer with λ_{exc} = 480 nm. Time-resolved transient absorption and fluorescence measurements were conducted using a pulsed YAG-OPO laser (λ_{exc} = 480 nm). High performance liquid chromatography (HPLC) was performed on a Hewlett-Packard 1050 HPLC.

Syntheses and Characterization. 5-bromo-1,10-phenanthroline (5-Br-phen). In a thick wall bomb flask equipped with a PTFE stopper and a magnetic stirring bar, 3.60 g (20.00 mmol) of anhydrous 1,10-phenanthroline (phen) were dissolved in 14 mL of fumic

H_2SO_4 (27–33% free SO_3) and the solution was treated with 0.60 mL (11.71 mmol) of bromine. The reaction mixture was then stirred for 14 hours at 120–125 ˚C upon which a color change from brown red to light orange red occurred. After cooling to room temperature, the reaction mixture was poured into 100 mL of ice water and the pH of the resulting yellow solution was adjusted to ca. 10–11 with conc. NH_3 solution upon which a dark red oil separated. The mixture was extracted three times with 100 mL CH_2Cl_2. The combined extracts were dried over anhydrous $MgSO_4$ and the solvent was removed in vacuo. The residual light purple solid was suspended in 400 mL of warm ether (ca. 30 ˚C) and the suspension was filtered through celite to yield a colorless filtrate which was brought to dryness in vacuo. 5-Bromo-1,10-phenanthroline was isolated as a colorless solid which was used without any further purification. Yield: 4.00 g (77%). ^{1}H NMR (300 MHz, $CDCl_3$): δ 9.06 (m, 2H), 8.49 (dd, J_a = 7.2 Hz, J_b = 1.2 Hz, 1H), 8.00 (dd, J_a = 8.1 Hz, J_b = 1.4 Hz, 1H), 7.94 (s, 1H), 7.58 (dd, J_a = 8.3 Hz, J_b = 4.1 Hz, 1H), 7.48 (dd, J_a = 8.1 Hz, J_b = 4.5 Hz, 1H). MS (ESI): *m/z* calculated for $C_{12}H_7N_2$ ($[M]^+$) 179.2, found 180.

5-(5-hydroxy-1-pentynyl)-1,10-phenanthroline. A solution of 8.00 g (30.90 mmol) of 5-Br-phen and 0.90 g (0.78 mmol) of $Pd(PPh_3)_4$ in 120 mL of pyrrolidine was treated with 3.30 mL (35.58 mmol) of 4-pentyn-1-ol and stirred for 10 hours at 75–80 ˚C. After cooling to room temperature, the mixture was poured into 250 mL of saturated aqueous NH_4Cl and extracted four times with 100 mL of CH_2Cl_2. The combined organic layers were washed with saturated aqueous NH_4Cl, saturated aqueous NaCl and dried over anhydrous $MgSO_4$. The solvent was removed in vacuo to leave a brown oily residue which was dissolved in 20 mL of $CHCl_3$. The solution was flash chromatographed on Al_2O_3 (neutral) using $CHCl_3$ as the eluant. The combined fractions were brought to dryness in vacuo and residual light yellow oil was diluted in ca. 15 mL of CH_2Cl_2. After evaporation of the latter in vacuo, the remaining light yellow solid was washed twice with 10 mL of hexanes and dried. Yield: 3.89 g (48%). ^{1}H NMR (300 MHz, $CDCl_3$): δ

9.10 (dd, J_a = 4.3 Hz, J_b = 1.5 Hz, 1H), 9.06 (dd, J_a = 4.5 Hz, J_b =1.5 Hz, 1H), 8.60 (dd, J_a = 8.3 Hz, J_b = 1.5 Hz, 1H), 7.83 (s, 1H), 7.58 (dd, J_a =8.3 Hz, J_b = 4.3 Hz, 1H), 7.51 (dd, J_a = 8.1 Hz, J_b = 4.5 Hz, 1H), 3.83 (t, J = 6.1 Hz), 2.65 (t, J = 7.1 Hz, 2H), 1.90 (m, 2H), 1.75 (s, 1H). MS (ESI): *m/z* calculated for $C_{17}H_{14}N_2O$ ($[M]^+$) 262.3, found 263.

5-(5-hydroxy-1-pentyl)-1,10-phenanthroline (phen'-OH). A mixture of 5.65 g (21.56 mmol) of 5-(5-hydroxy-1-pentynyl)-1,10-phenanthroline, 4.0 g of Pd/C (10%), 50 mL of 10% aqueous HCl and 200 mL of MeOH was stirred under a hydrogen atmosphere for 48 hours at room temperature. After an atmosphere of argon was reestablished, the reaction mixture was filtered through celite and the organic solvent was removed in vacuo. The residue was diluted with 50 mL of H_2O, and the pH was adjusted to ca. 11.5 with 10% aqueous NaOH. After extraction of the aqueous layer with CH_2Cl_2 (five times with 100 mL), the combined extracts were washed with water, dried over anhydrous $MgSO_4$, filtered, and brought to dryness in vacuo. A light yellow residue was obtained which was washed twice with 5 mL of diethyl ether and dried. Yield: 4.40 g (77%). ^{1}H NMR (300 MHz, $CDCl_3$): δ 9.07 (dd, J_a = 4.2 Hz, J_b = 1.5 Hz, 1H), 9.00 (dd, J_a = 4.3 Hz, J_b = 1.6 Hz, 1H), 8.30 (dd, J_a = 8.4 Hz, J_b = 1.5 Hz, 1H), 8.04 (dd, J_a =8.1 Hz, J_b = 1.5 Hz, 1H), 7.54 (dd, J_a = 8.4 Hz, J_b = 4.2 Hz), 7.49 (m, 2H), 3.58 (m, 2H), 3.00 (t, J = 7.5 Hz), 1.77–1.41 (m, 7H). MS (ESI): *m/z* calculated for $C_{17}H_{18}N_2O$ ($[M]^+$) 266.3, found 267.

5-(4-methoxycarbonyl-butyl)-1,10-phenanthroline (phen'-OMe) A suspension of 4.40g (16.35mmol) of phen'-OH in 300 mL of acetone was treated with 10.07 g (63.72 mmol) of $KMnO_4$ and stirred for 3 hours at room temperature upon which a brown precipitate formed. The resulting reaction mixture was brought to dryness in vacuo and the residue was suspended in 200 mL of H_2O. The dark brown suspension was treated with 15 mL of 10% aqueous NaOH and heated to reflux for 15 min. After cooling to room temperature, the black slurry was filtered through celite and the residue was washed with 20 mL of 0.1 N aqueous NaOH. The combined filtrates were extracted twice with

80 mL of CH_2Cl_2 to remove organic impurities. The pH of the aqueous layer was adjusted to 3–4 with conc. aqueous HCl and the solvent was carefully removed in vacuo. The remaining viscous residue was suspended in 300 mL of MeOH and the suspension was treated dropwise with conc. H_2SO_4 until the formation of an off white precipitate stopped. The slurry was filtered and the residue was washed twice with 10 mL of MeOH. The combined filtrates were treated with ca. 1mL of conc. H_2SO_4 and heated to reflux for 3 hours. After cooling to room temperature, the mixture was concentrated to ca. 10mL, and the concentrate was suspended in 200 mL of H_2O. After the pH was adjusted to ca. 8 with 10% aqueous NaOH, the suspension was extracted six time with 100 mL of CH_2Cl_2. The combined organic extracts were washed with aqueous NaCl, dried over anhydrous $MgSO_4$ and brought to dryness in vacuo to leave an orange-yellow oil. This was dissolved in 10 mL of CH_2Cl_2/MeOH (20:1), and the solution was flash chromatographed on silica with CH_2Cl_2/MeOH (20:1) as the eluant. The corresponding fractions were combined, and the solvent was removed in vacuo. The residue was recrystallized from boiling ethyl acetate. At -20 ºC, light yellow crystals precipitated which were separated from the mother liquor, washed with 10 mL of ethyl acetate and 20 mL of hexanes and dried. Yield: 1.41 g (30%). ^{1}H NMR (500 MHz, $CDCl_3$): δ 9.18 (d, J = 4.0 Hz, 1H), 9.12 [d, J = 3.0 Hz, 1H), 8.40 (d, J = 8.5 Hz, 1H), 8.15 (d, J = 8.0Hz, 1H), 7.65 (dd, J_a = 8.5 Hz, J_b = 4.0Hz, 1H), 7.58 (m, 2H), 3.65 (s, 3H), 3.13 (t, J = 6.5 Hz, 2H), 2.39 (t, J = 7.0 Hz, 2H), 1.82 (m, 4H). MS (ESI): *m/z* calculated for $C_{18}H_{18}N_2O_2$ ($[M]^+$) 294.3, found 295.

$[Ru(CO)_2(phen)(phen'\text{-}OMe)](PF_6)_2$ A suspension of 511mg (0.80 mmol) of $[Ru(CO)_2(phen)Cl_2]$ and 298mg (1.02 mmol) of phen'-OMe in 30 mL of 2-methoxy-ethanol was heated to reflux for 2 hours. A change of color from yellow to orange-yellow occurred. After the reaction mixture was cooled to room temperature, a ca. 25% aqueous solution of NH_4PF_6 was added dropwise until the precipitation of a yellow solid was completed. The latter was filtered, washed five times with 10 mL portions of water

and five times with 20 mL portions of diethyl ether. The precipitate was isolated as a shiny yellow solid and used without further purification. Yield: 0.37 g (50%). ^{1}H NMR not taken. MS (ESI): *m/z* calculated for $C_{32}H_{26}F_6N_4O_4PRu$ ($[M\text{-}PF_6]^+$) 776.6, found 777; *m/z* calculated for $C_{30}H_{26}F_6N_4O_2PRu$ ($[M\text{-}(CO)_2\text{-}PF_6]^+$) 720.6, found 721; *m/z* calculated for $C_{28}H_{20}F_6N_4O_2PRu$ ($[M\text{-}(CH_2CHCOOCH_3)\text{-}PF_6]^+$) 690.5, found 691.

Synthesis of [Ru(phen)(5-phen'-OMe)(dppz)]Cl$_2$. A solution of 464 mg (0.50 mmol) of $[Ru(CO)_2(phen)(phen'\text{-}OMe)](PF_6)_2$, 284 mg (1.00 mmol) of dppz, and 146 mg (2.86 mmol) of trimethylamine-N-oxide (TMNO) in 20 mL of 2-methoxyethanol was heated to reflux for 2 hours. A rapid change of color from orange yellow to dark red occurred. After cooling to room temperature, the crude reaction mixture was absorbed on pre-equilibrated Sephadex QAE-A25 anion exchange resin. With water as eluant, an orange red fraction was obtained which was brought to dryness in vacuo. The residue was dissolved in 20 mL of acetonitrile and the solution was chromatographed on $A1_2O_3$ (neutral). With MeCN/H_2O (50: 1), a bright yellow fraction of side products was eluted; whereas, the desired product was obtained with MeCN/H_2O (94:6). The corresponding orange-red fraction was brought to dryness in vacuo to yield a dark red crystalline solid. Yield: 290 mg (62%). ^{1}H NMR (500 MHz, CD_3OD): δ 9.63 (m, 2H), 8.91 and 8.89 (both d, J = 8.5 Hz), 8.76 (m, 2H), 8.68 (d, J = 9.0 Hz, 0.5H), 8.66 (d, J = 8.5 Hz, 0.5H), 8.43–8.34 (m, 7H), 8.24 (m, 2H), 8.21 (m, 0.5H), 8.17 (m, 1H), 8.10 (dd, J_a = 5.5 Hz, J_b = 1.0 Hz, 0.5H), 8.07 (dd, J_a = 6.5 Hz, J_b = 3.5 Hz, 2H), 7.88–7.77 (m, 5H), 7.74 (dd, J_a = 8.5 Hz, J_b = 5.5 Hz, 1H), 3.65, 3.64 (both s, 3H), 3.38 (t, J = 7.5 Hz, 2H), 2.46 (m, 2H), 1.93 (m, 2H), 1.85 (m, 2H). MS (ESI): *m/z* calculated for $C_{48}H_{36}N_8O_2Ru$ ($[M]^{2+}$) 428.9, found 429; *m/z* calculated for $C_{42}H_{26}N_8Ru$ ($[M\text{-}(CH_2CHCH_2CH_2COOCH_3)]^{2+}$) 371.9, found 372.

Synthesis of [Ru(phen)(5-phen')(dppz)]Cl$_2$ A solution of 281 mg (0.30 mmol) of $[Ru(phen)(5\text{-}phen'\text{-}OMe)(dppz)]Cl_2$ in 20 mL of water was treated with 840 mg (20 mmol) of LiOH and stirred for 16 hours at room temperature upon which an orange-red

precipitate formed. The mixture was diluted with 50 mL of water, and the pH was adjusted to 5.5 with 1.0 M aqueous HCl. After addition of 400 mL of water and 5 mL of MeCN, the resulting solution was loaded on a C18 Sep-Pak column (5 g) and the adsorbed product was washed 20 times with 20 mL portions of water to remove residual salts. With MeCN/trifluoroacetic acid (0.1%) (9:1) as the eluant, an orange-red fraction was obtained which was brought to dryness in vacuo. Yield: 250 mg (90%). ^{1}H NMR (500 MHz, CD_3OD): δ 9.77 (m, 2H), 8.88 and 8.87 (both d, J = 1.0 Hz, 1H), 8.71 (m, 2H), 8.63 (dd, J_a = 8.0 Hz, J_b =1.0 Hz, 0.5H), 8.62 (dd, J_a = 8.5 Hz, J_b = 1.0 Hz, 0.5 H), 8.51 (dd, J_a = 6.0 Hz, J_b = 3.0 Hz, 2H), 8.34 (m, 4.5H), 8.27 (dd, J_a = 5.0 Hz, J_b = 1.0 Hz, 0.5H), 8.19 (m, 2H), 8.14 (dd, J_a = 6.0 Hz, J_b = 3.0 Hz, 2H), 8.11 (m, 1.5H), 8.05 (dd, J_a = 5.0 Hz, J_b = 1.0 Hz, 0.5H), 7.87 (m, 2H), 7.79–7.71 (m, 3H), 7.69 (dd, J_a = 8.0 Hz, J_b = 5.0 Hz, 1H), 3.37 (t, J = 7.5 Hz, 2H), 2.41 (m, 2H), 1.94 (m, 2H), 1.83 (m, 2H). MS (ESI): *m/z* calculated for $C_{47}H_{33}N_8O_2Ru$ ($[M-H]^+$) 843, found 843; *m/z* calculated for $C_{47}H_{34}N_8O_2Ru$ ($[M]^{2+}$) 422, found 422. UV-visible data (H_2O): 266 nm (ε = 1.2 ×10^5 M^{-1}cm^{-1}), 374 nm (ε = 2.2 ×10^4 M^{-1}cm^{-1}), 442 (ε = 2.1 ×10^4 M^{-1}cm^{-1}).

[Ru(bpy)$_2$bpy']-DNA conjugate synthesis. [Ru(bpy)$_2$bpy']Cl_2 (bpy'=4-butyric acid-8'-methyl bipyridyl) was prepared according to published procedures.[12] The acid was coupled to amine-modified DNA as previously described.[18] The conjugate was cleaved from the resin with aqueous ammonia at 55 °C for 8 hours. Subsequent reverse phase HPLC (0–35% CH_3CN over 50 minutes, Rainin Dynamax C4 column) afforded a diastereomeric mixture of the desired [Ru(bpy)$_2$bpy']-DNA conjugate. The conjugate was quantitated using ε_{452} = 1.46 ×10^4 M^{-1}cm^{-1}. MS (MALDI-TOF): *m/z* calculated for $[M+H]^+$ 5053.9, found 5054.2.

Methods. Sample Preparation. Unless otherwise noted, all experiments were performed in a buffer of 5 mM sodium phosphate (NaPi), 50 mM sodium chloride (NaCl), at pH=7. Ruthenium-modified and 7-deazaguanine containing duplexes were synthesized as previously described.[1,18] All conjugates were purified by reverse phase

HPLC (0–35% CH_3CN over 50 minutes, Rainin Dynamax C4 column). Duplexes were created by hybridizing the appropriate amounts of complementary single strands based on the extinction coefficients for ruthenium-modified sequences (ε_{440} = 21000 $M^{-1}cm^{-1}$) and calculated extinction coefficients for unmodified sequences (ε_{260} ($M^{-1}cm^{-1}$): dC = 7400; dT = 8700; dG = 11,500; dA = 15,400; dZ = 10,500.[1a,19,20] Characterization for all oligonucleotides included MALDI-TOF mass spectrometry and UV-visible spectroscopy.

Steady-state Spectroscopy. All samples were purified via HPLC and de-salted prior to use. Emission and excitation spectra were obtained on an ISS K2 spectrofluorometer. Emission intensities were determined by integration of the luminescence spectrum and standardized against $[Ru(bpy)_3]Cl_2$ as a calibration for the instrument. Solutions containing 5 μM Ru-DNA duplex were excited at 480 nm, and emission was monitored from 500 nm to 800 nm. Excitation spectra were obtained by monitoring at the emission maximum while varying excitation wavelength from 350 nm to 600 nm.

Time-resolved Spectroscopy. All Ru-DNA conjugates were purified via HPLC and de-salted prior to use. Time-resolved transient absorption and fluorescence measurements were conducted using a pulsed YAG-OPO laser (λ_{exc} = 480 nm). Laser powers ranged from 2 to 4 mJ/pulse. The Ru-DNA concentration in all samples was 5 μM. The buffer used in both fluorescence and transient absorption measurements was 5 mM NaPi, 50 mM NaCl, pH=7. Decays were fit to biexponential curves using in-house software and least-squares analysis.

4.3 Results and Discussion

4.3.1 Synthesis of ruthenium-DNA conjugates

Ruthenium(II) Intercalator. The architecture of $[Ru(phen)_2dppz]^{2+}$ must be modified in order to be able to covalently tether it to the end of a DNA oligonucleotide. It is also important that any modifications do not drastically alter the binding, photo-

physical, and electrochemical properties of the intercalator compared to its parent complex. The ruthenium(II) complex we created that satisfies these requirements is shown in Figure 4.4. To synthesize the molecule we sequentially attached the three polypyridyl ligands to the ruthenium metal center according to a method developed by Anderson et al.[17] (details given in the Experimental Section). The method, which is a general route to creating ruthenium complexes with three different polypyridyl ligands, allowed us to create a new metal complex ([Ru(phen)(phen')dppz]$^{2+}$) very similar in structure to the well-characterized [Ru(phen)$_2$dppz]$^{2+}$. The three different ligands all play critical roles in how the complex behaves when attached to DNA. The dipyridophenazine ligand (dppz) intercalates into DNA and provides intimate interaction with the base stack, a requirement for observing fast and efficient DNA-mediated charge transfer. The modified phenanthroline (phen'), in addition to providing the photophysical properties typical of ruthenium(II) polypyridyls, allows the complex to be attached to the end of a modified DNA oligonucleotide (*vide infra*). The unmodified phenanthroline (phen) ligand serves to complete the kinetically inert ruthenium(II) coordination sphere and provides desirable spectroscopic properties.

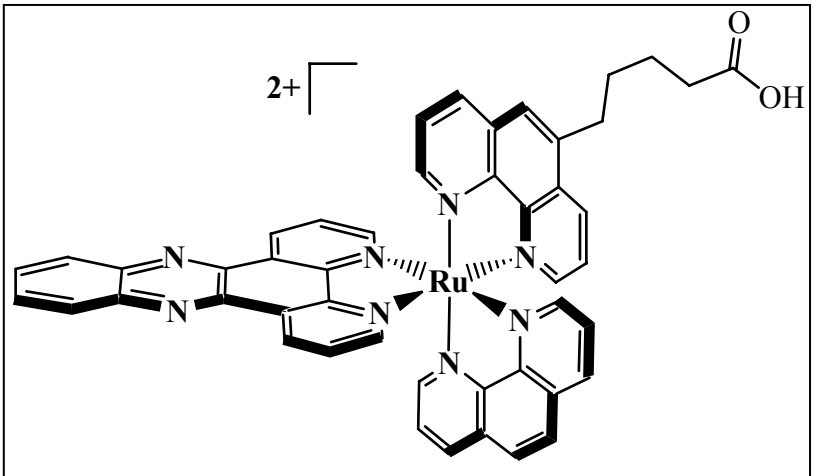

Figure 4.4 Structure of [Ru(phen)(phen')dppz]$^{2+}$.

A modified 1,10-phenanthroline (phen') was chosen instead of a modified 2,2'-bipyridine (bpy' = 4-butyric acid-8'-methyl bipyridyl) based on previous results from our laboratory. Ruthenium conjugates utilizing bpy' instead of phen' showed little or no fluorescence quenching by 7-deazaguanine, even at short donor-acceptor separations. Distance dependent fluorescence quenching was notably absent, and the observed fluorescence varied little with the chosen DNA sequences. Further, hypochromism upon DNA binding was reduced relative to the parent complex (without the linker arm), indicating the complex was not well stacked within the DNA helix. The phen'-based ruthenium intercalator did not suffer from these drawbacks, and that is the complex we used to generate the results detailed in this Chapter.

Ruthenium-DNA oligonucleotides. After synthesizing the desired ruthenium(II) intercalator, we set about attaching it to the end of DNA. The synthesis of ruthenium-containing DNA oligonucleotides was performed as outlined previously[18] and is summarized in Figure 4.5. The desired single strand sequence was synthesized on an automated DNA synthesizer and the trityl protecting group removed to leave a 5'-OH on the terminal nucleotide on the controlled pore glass (CPG) resin. This was reacted with carbonyl diimidazole followed by a diaminoalkane to form an amine terminated oligonucleotide (still attached to the CPG). Next, $[Ru(phen)(phen')dppz]^{2+}$, with the carboxylic acid group on the phen' ligand, was coupled to the amine to create a Ru-DNA conjugate (still attached to the CPG). This was cleaved from the resin and deprotected in aqueous ammonia and purified via HPLC to give the desired single strand Ru-DNA conjugate. Ru-DNA single strands and their G or Z containing complements were then quantitated by UV-visible spectroscopy, and the appropriate amounts were annealed to create Ru/G- and Ru/Z-modified DNA duplexes.

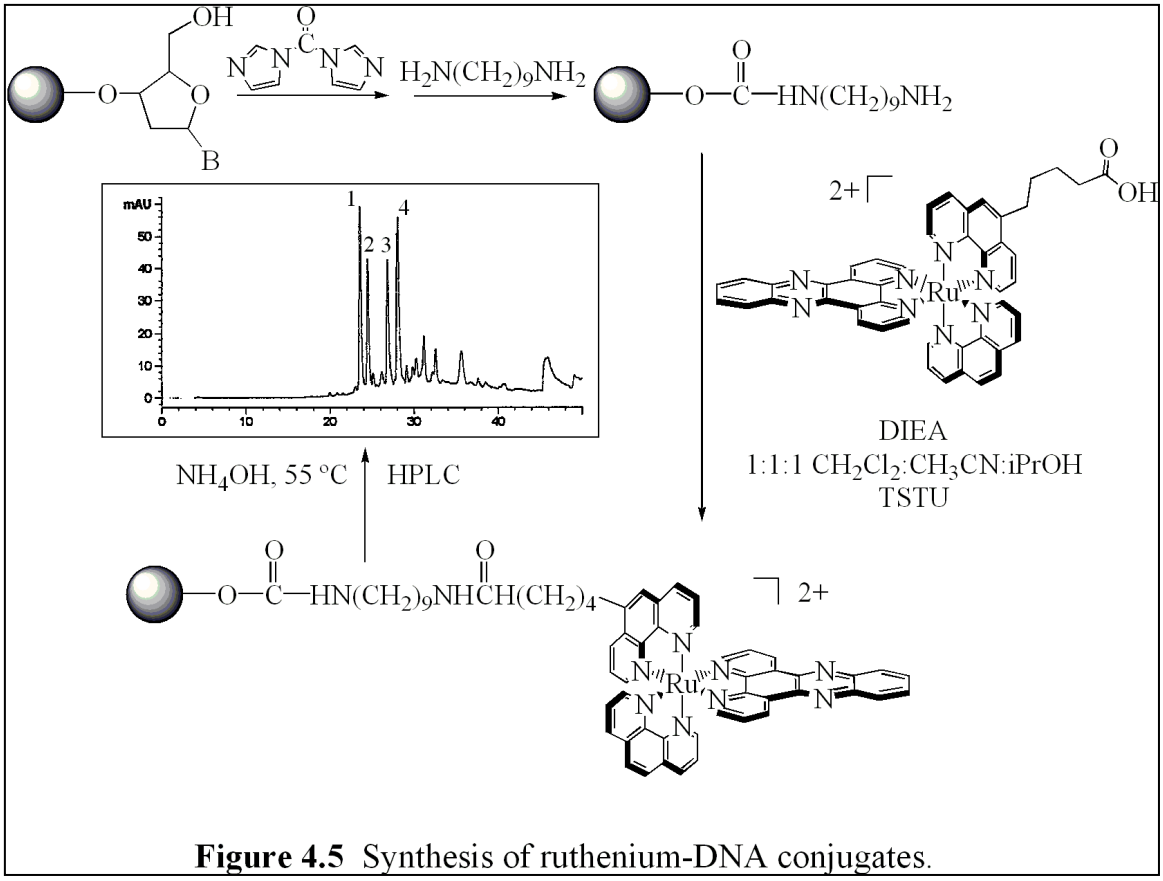

Figure 4.5 Synthesis of ruthenium-DNA conjugates.

Inspection of the HPLC traces (example shown in Figure 4.5) reveals four main peaks that elute with retention times similar to what we would expect for metallointercalator-DNA conjugates. MALDI-TOF mass spectrometry analysis revealed the peaks all had the same (expected) mass for the given Ru-DNA sequence (Table 4.1), and UV-visible spectra showed the transitions consistent with the presence of both ruthenium(II) (broad MLCT band in the 400–500 nm region)[5] and DNA (large π-π* transition at 260 nm).[19,20] Thus, the peaks have the same underlying composition.

Closer examination of the $[Ru(phen)(phen')dppz]^{2+}$ structure provides the reason for multiple HPLC peaks when the complex is attached to DNA. Shown in Figure 4.6 are the structures of the various diastereomers of the intercalator when tethered to a DNA oligonucleotide. There are Δ and Λ configurations about the metal center, and each of those configurations can have the linker arm on the phen' in an axial or equatorial

position.[21] It is really quite remarkable that the subtle differences in structure allow all of the Ru-DNA diastereomers to be separated and isolated via HPLC with a non-chiral stationary phase.

HPLC Peak (Fig. 4.5)	*m/z* calculated (amu)	*m/z* found (amu)
1	5227.2	5226.2
2	5227.2	5227.5
3	5227.2	5227.4
4	5227.2	5228.8

Table 4.1 Mass spectrometry data for the Ru-DNA conjugates indicated by peaks 1–4 in the HPLC trace in Figure 4.5.

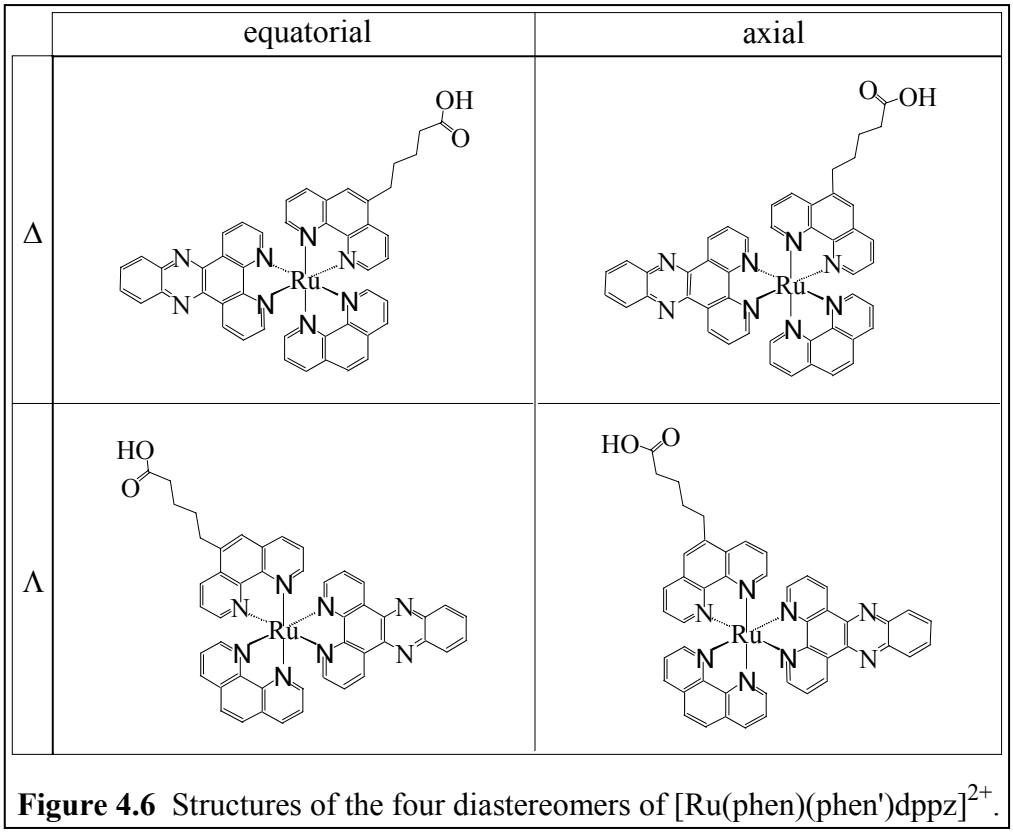

Figure 4.6 Structures of the four diastereomers of $[Ru(phen)(phen')dppz]^{2+}$.

In order to verify that the four isolated HPLC peaks contained two Δ and two Λ strands we performed circular dichroism measurements. Figure 4.7 shows the spectra of the four peaks isolated from the HPLC shown in Figure 4.5. Assignments of the configuration about the metal center were made by comparing the signals to the known circular dichroism spectra of Δ and Λ $[Ru(phen)_2dppz]^{2+}$.[22,23] As expected, the signals provide solid evidence that the four peaks correspond to two Δ plus two Λ Ru-DNA diastereomers. In going forward with our studies, we will examine only DNA sequences in which all four of the diastereomers can be separated via HPLC. This will allow us to isolate the effect of intercalator chirality on DNA-mediated charge transfer.

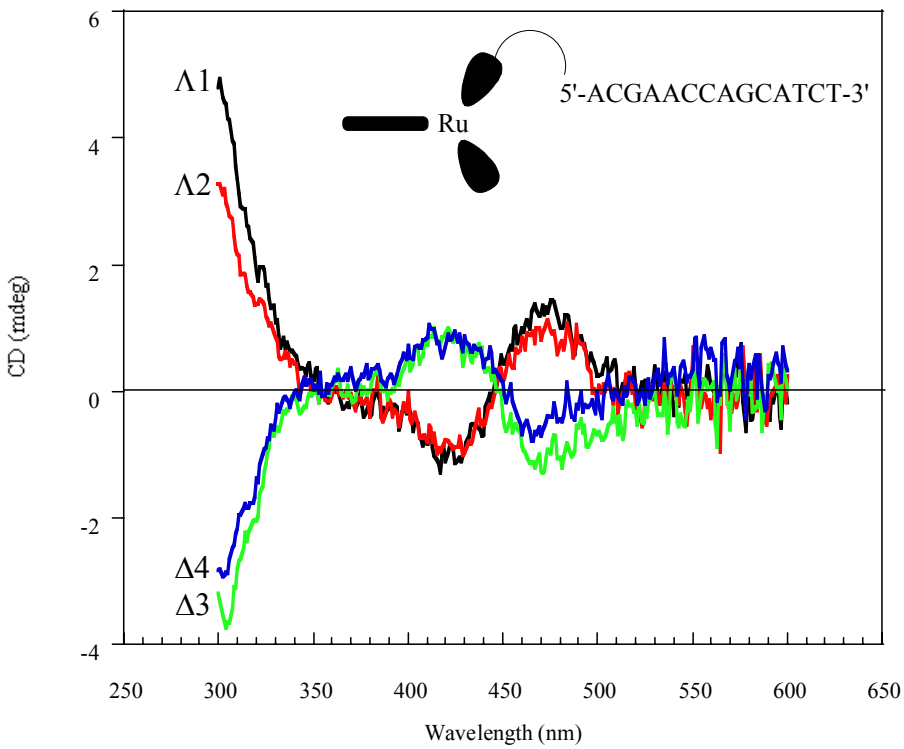

Figure 4.7 Circular dichroism spectra of the four $[Ru(phen)(phen')dppz]^{2+}$-DNA conjugates (sequence shown in the Figure) isolated from the HPLC trace shown in Figure 4.5. Spectra taken in H_2O at ambient temperature, with sample concentrations of approximately 5 μM.

4.3.2 Steady-state spectroscopy of Ru/G and Ru/Z conjugates

Ruthenium-DNA Assemblies. The Ru-DNA duplexes assemblies employed in our studies are shown in Figure 4.8. The donor-acceptor distances (7–14 Å) are worst-case estimates based on intercalation of the ruthenium complex between the third and fourth base pairs. Molecular modeling indicates the linker attaching the complex to the DNA backbone will not allow intercalation at a site farther down the helix without significantly disrupting the structure of the duplex. Spectroscopy experiments were performed on all four of the Ru-diastereomers (for both Ru/G and Ru/Z duplexes) at each donor-acceptor distance. Unfortunately, other sequences did not give rise to separation of all the diastereomers via HPLC, so the sequences shown in Figure 4.8 are the only ones we studied.

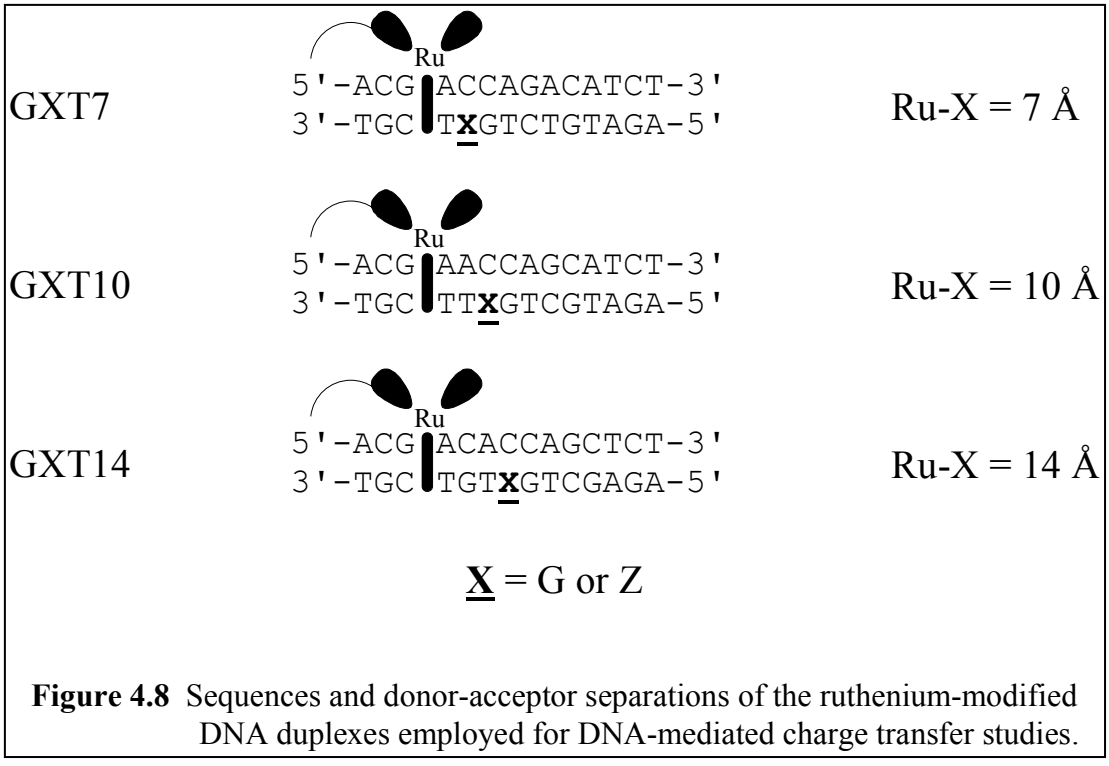

Figure 4.8 Sequences and donor-acceptor separations of the ruthenium-modified DNA duplexes employed for DNA-mediated charge transfer studies.

Fluorescence Behavior. Figure 4.9 shows the fluorescence spectra for select G and Z containing, Ru-modified DNA duplexes. The single atom change in going from G to Z results in a substantial amount of ruthenium luminescence quenching. The quantum yields and quenching values for the series of duplexes outlined in Figure 4.8 are summarized in Table 4.2. Steady-state luminescence quenching in the 7-deazaguanine containing duplexes is readily apparent at donor-acceptor separations of 7–14 Å. After 14 Å, the amount of ruthenium luminescence quenching by 7-deazaguanine is negligible. Additionally, absolute quenching yields are higher for the Δ isomers than the Λ isomers of the ruthenium-DNA conjugates. This is in agreement with how well the tethered isomers are expected to intercalate into the DNA base stack.[24] The thermodynamic driving force for the reaction is the same in all cases, so the observed differences really emphasize the importance of stacking on charge transfer mediated by the DNA double helix.

The distance dependence of the quenching reaction is shallow and depends on the chirality of the tethered metallointercalator. The distance dependences (0.3 $Å^{-1}$ for the Λ isomer and 0.5 $Å^{-1}$ for the 0.3 $Å^{-1}$ isomer) are similar to those obtained in previous studies examining photoinduced DNA-mediated charge transfer between fluorophores and 7-deazaguanine (Chapters 2 and 3). Surprisingly, the distance dependence is more shallow for the Λ isomer than the Δ isomer (Figure 4.10). This is in direct conflict with how well the intercalator is expected to bind to DNA, as Δ isomers show enhanced binding relative to Λ isomers because the ancillary ligands are able to fit in the DNA groove without steric clashing with the DNA backbone.[24] The reasons for our anamolous data are unclear but may be related to how the stacking of the reactants changes as the donor-acceptor distance increases.

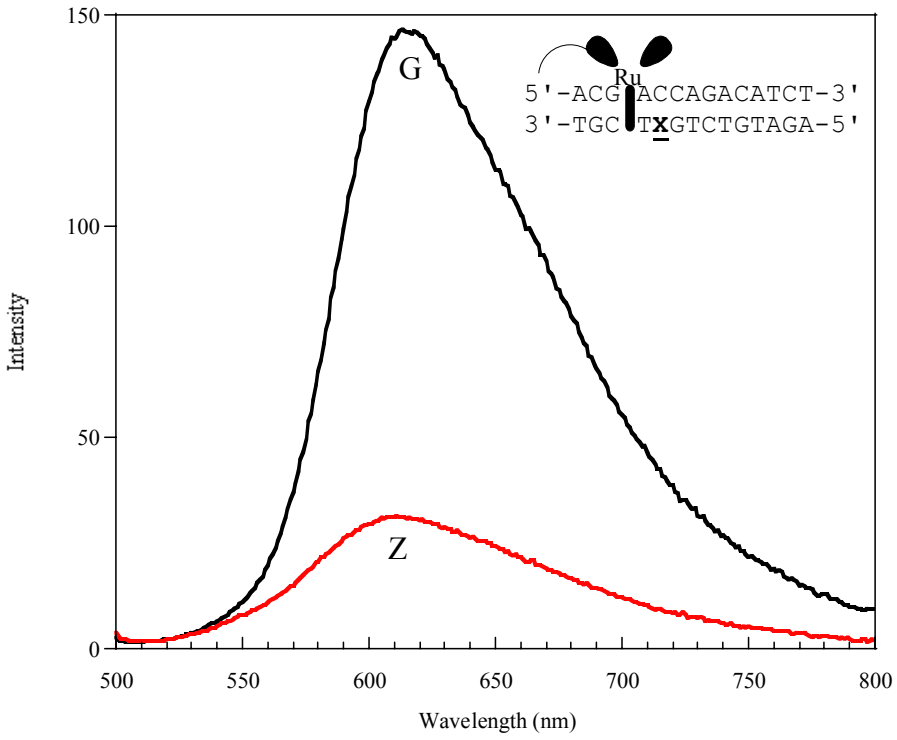

Figure 4.9 Steady-state fluorescence spectra of the G and Z containing, ruthenium-modified DNA duplexes shown in the Figure. Spectra shown are for the Δ4 diastereomer. λ_{exc}=480 nm. 5 μM duplex in 5 mM NaPi, 50 mM NaCl, pH=7 buffer.

Sample[a]	Δ/Λ[b]	I_G[c]	I_Z[d]	Fq[e]
GXT7 1	Λ	0.31	0.16	0.48
GXT10 1	Λ	0.25	0.22	0.14
GXT14 4	Λ	0.36	0.33	0.09
GXT7 2	Λ	0.22	0.11	0.49
GXT10 2	Λ	0.26	0.19	0.27
GXT14 3	Λ	0.67	0.61	0.09
GXT7 3	Δ	0.50	0.09	0.82
GXT10 3	Δ	0.33	0.23	0.30
GXT14 1	Δ	0.90	0.80	0.11
GXT7 4	Δ	0.42	0.16	0.63
GXT10 4	Δ	0.32	0.24	0.24
GXT14 2	Δ	0.88	0.83	0.06

Table 4.2 Steady-state fluorescence data for Ru/G and Ru/Z modified DNA duplexes. (a) Sequence and HPLC peak number of the Ru-DNA conjugate. (b) Chirality about the metal center of the Ru-DNA conjugate. (c) Relative quantum yield of Ru/G modified duplexes. (d) Relative quantum yield of Ru/Z modified duplexes. (e) The fraction of luminescence quenched (Fq). Experimental conditions: 5 μM DNA duplex in 5 mM NaPi, 50 mM NaCl, pH=7.0 buffer with λ_{exc} = 480 nm and λ_{obs} = 500–800 nm. Calculated intensities are relative to a 10 μM $[Ru(bpy)_3]^{2+}$ in water standard.

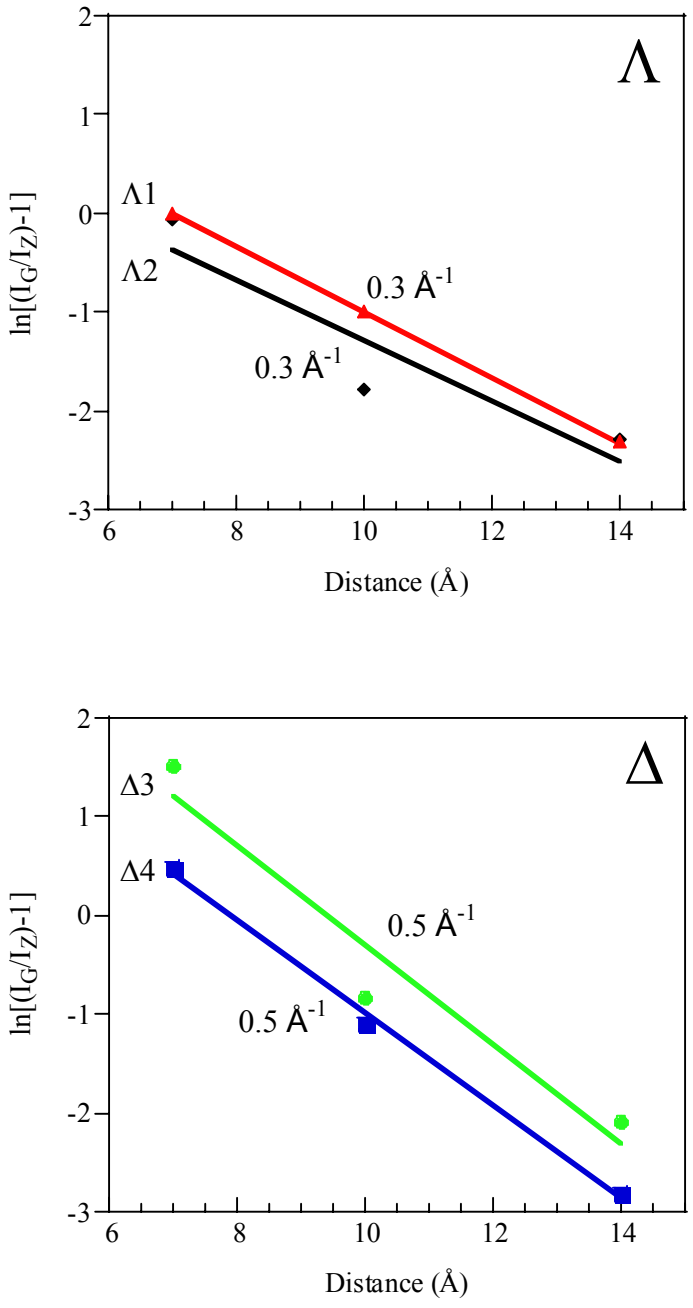

Figure 4.10 Distance dependences of DNA-mediated charge transfer quenching yields between *Ru and 7-deazaguanine for Λ (top) and Δ (bottom) Ru-DNA diastereomers.

Control Experiments. To verify that intercalation was essential for observing DNA-mediated charge transfer in Ru/Z DNA conjugates, we created a DNA duplex that contained a non-intercalating ruthenium(II) complex (Figure 4.11). The new metal complex consists of an architecture of 2,2'-bipyridines, ligands that do not intercalate into DNA. The photophysical properties, however, are very similar to that of our intercalator.

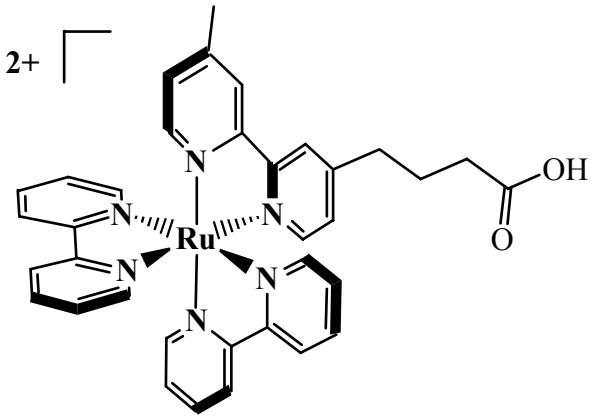

Figure 4.11 Structure of the non-intercalating $[Ru(bpy)_2(bpy')]^{2+}$.

Figure 4.12 shows the fluorescence spectra for the Ru/G- and Ru/Z-modified duplexes created using $[Ru(bpy)_2bpy']^{2+}$. The sequence is the same as that used for the shortest donor-acceptor separation in the intercalative Ru/Z duplexes (7 Å). As is readily apparent from the Figure, the luminescence of the non-intercalating compound is not quenched by 7-deazaguanine in DNA. This allows us to conclude two things: (1) intercalation is necessary to observe DNA-mediated photoinduced charge transfer between *Ru(II) and Z, and (2) direct contact of the metal complex with the 7-deazaguanine is unlikely and thus cannot be used to explain the efficient quenching behavior. This further demonstrates that intimate access of the reactants to the DNA π stack is essential for observing efficient charge transfer through the double helix.

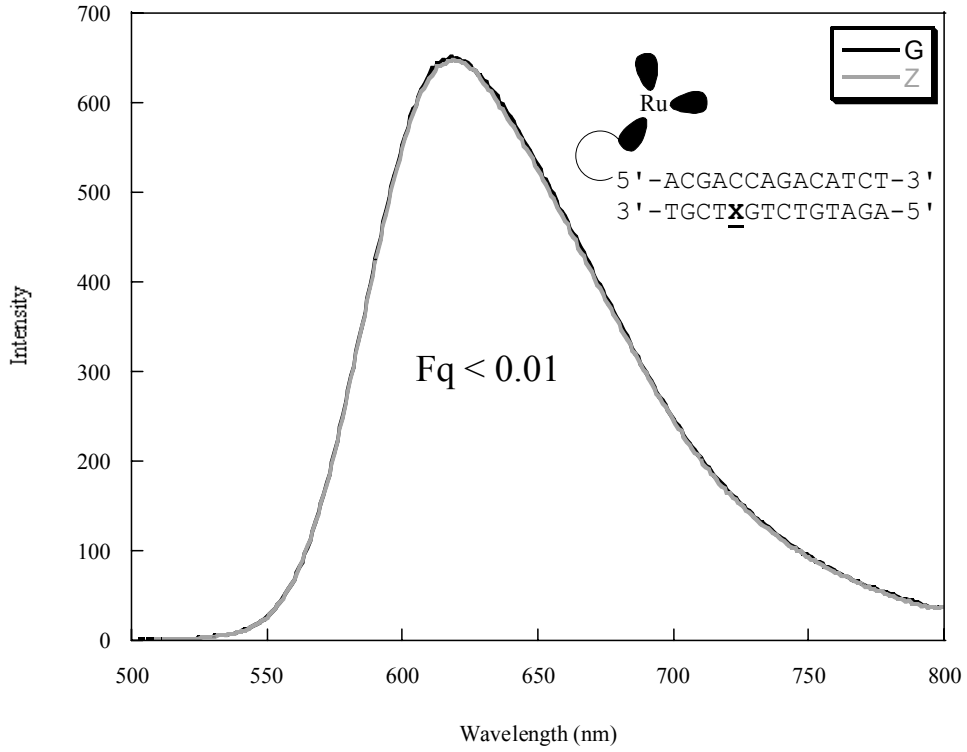

Figure 4.12 Steady-state fluorescence spectra of the G (black) and Z (gray) containing, $[Ru(bpy)_2(bpy')]^{2+}$-modified DNA duplexes shown in the Figure. Spectra shown are for the racemic conjugate. λ_{exc}= 480 nm. 10 μM duplex in 5 mM NaPi, 50 mM NaCl, pH=7.0 buffer. Total luminescence quenching is less than 1%.

4.3.3 Time-resolved spectroscopy of Ru/G and Ru/Z conjugates

Fluorescence. Steady-state quenching for all the diastereomers was easily characterized over a range of donor-acceptor distances. The reaction exhibited a shallow distance dependence that was found to depend on the configuration about the metal center of the Ru-DNA conjugate. What, then, are the dynamics of this quenching process? Figures 4.13–4.16 illustrate the time-resolved fluorescence decays for all the diastereomers of the Ru/G- and Ru/Z-modified duplexes with donor-acceptor separations ranging from 7–14 Å. The key lifetime parameters derived from these spectra are summarized in Table 4.3.

The decay of *Ru(II) in all cases is best fit with a biexponential function, consistent with the intercalators binding to the DNA double helix.[25] Because of low quenching yields, the decays at 10 and 14 Å donor-acceptor separations are similar for the Ru/G and Ru/Z pair for each diastereomer conjugate. The behavior at Ru-Z distances of 7 Å, however, is quite revealing. In the Δ-Ru/Z assemblies, the quenching is mostly static (i.e., the dynamics are not able to be resolved within the time response of the instrument, ca. 20 ns). In the Λ-Ru/Z assemblies, the quenching is mostly dynamic, with the data indicating quenching rate constants of ca. 185 ns for the Λ1-Ru/Z and ca. 128 ns for the Λ2-Ru/Z diastereomers. Unfortunately, the similarities in the Ru/G and Ru/Z traces at longer distances do not allow for a distance dependence analysis of the quenching rate.

How can we rationalize this behavior? The Δ-Ru complexes are expected to intercalate more deeply into the DNA helix than their Λ counterparts. This deeper intercalation provides better electronic access to the π stack of DNA. This leads to efficient electronic coupling between the donor and acceptor in the Δ-Ru/Z conjugates, which manifests itself as rapid photoinduced charge transfer. Similar behavior is observed when other reactants, such as ethidium (Chapter 2) and 2-aminopurine (Chapter 3), are well coupled to 7-deazaguanine through the DNA double helix. The ruthenium

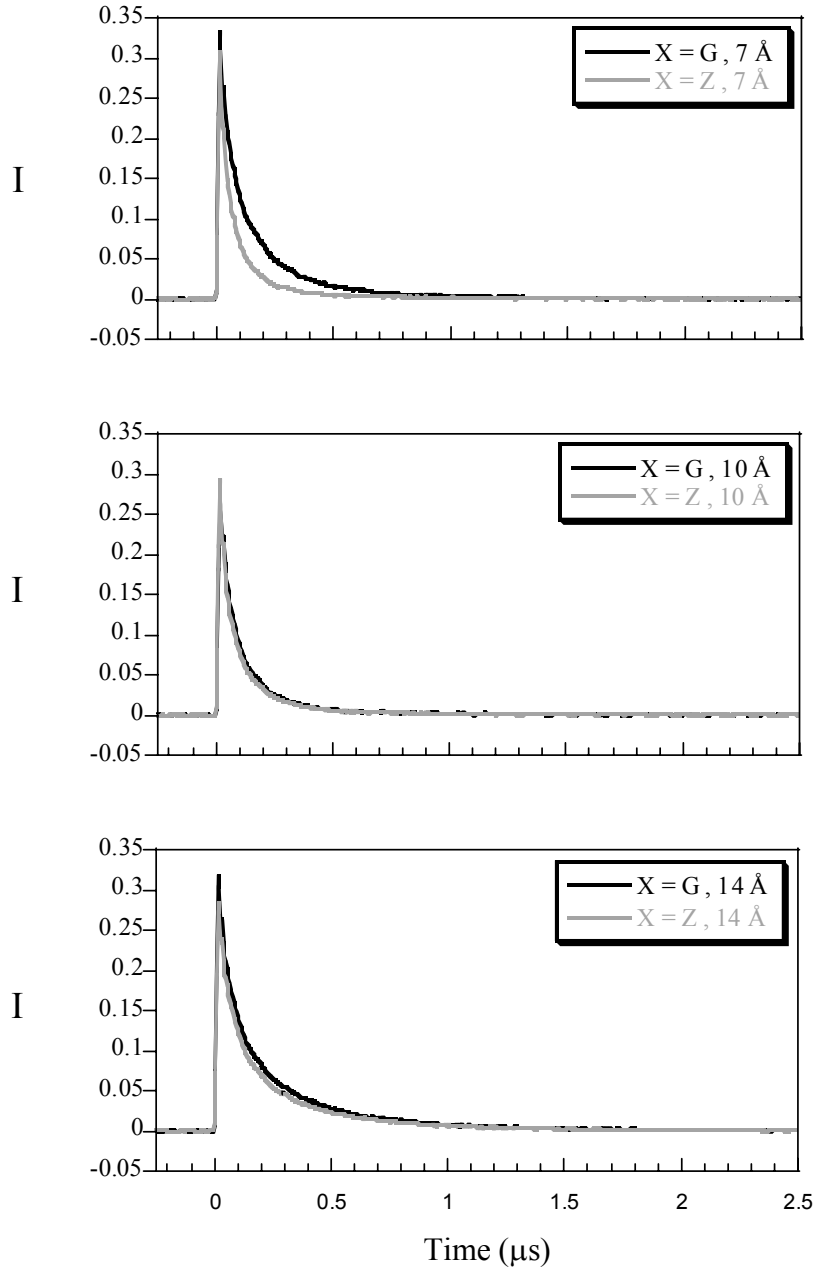

Figure 4.13 Time-resolved fluorescence of the G (black) and Z (gray) containing, $[Ru(phen)(phen')dppz]^{2+}$-modified DNA duplex series Λ1. Donor-acceptor distances are given in the Figure. λ_{exc}=480 nm, λ_{obs}=610 nm. 5 μM duplex in 5 mM NaPi, 50 mM NaCl, pH=7 buffer.

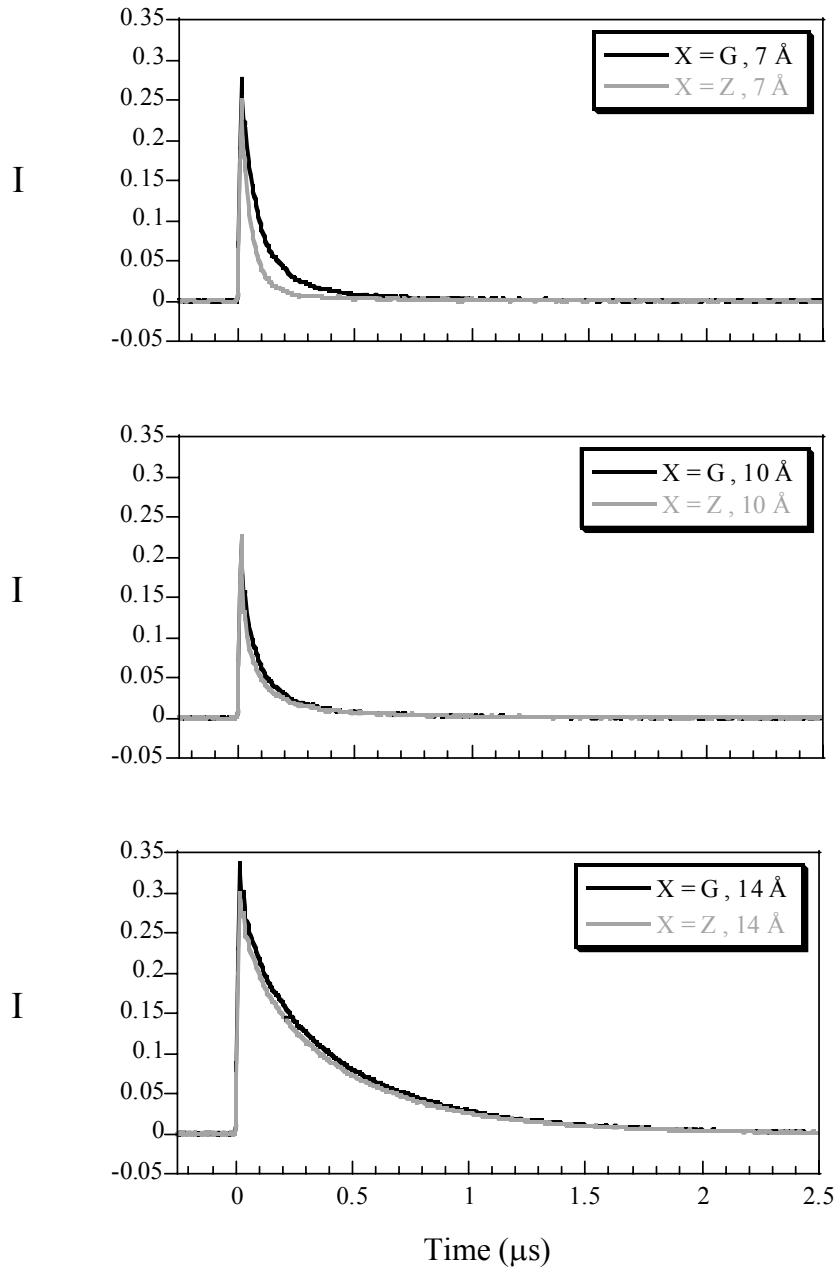

Figure 4.14 Time-resolved fluorescence of the G (black) and Z (gray) containing, $[Ru(phen)(phen')dppz]^{2+}$-modified DNA duplex series Λ2. Donor-acceptor distances are given in the Figure. λ_{exc}=480 nm, λ_{obs}=610 nm. 5 μM duplex in 5 mM NaPi, 50 mM NaCl, pH=7 buffer.

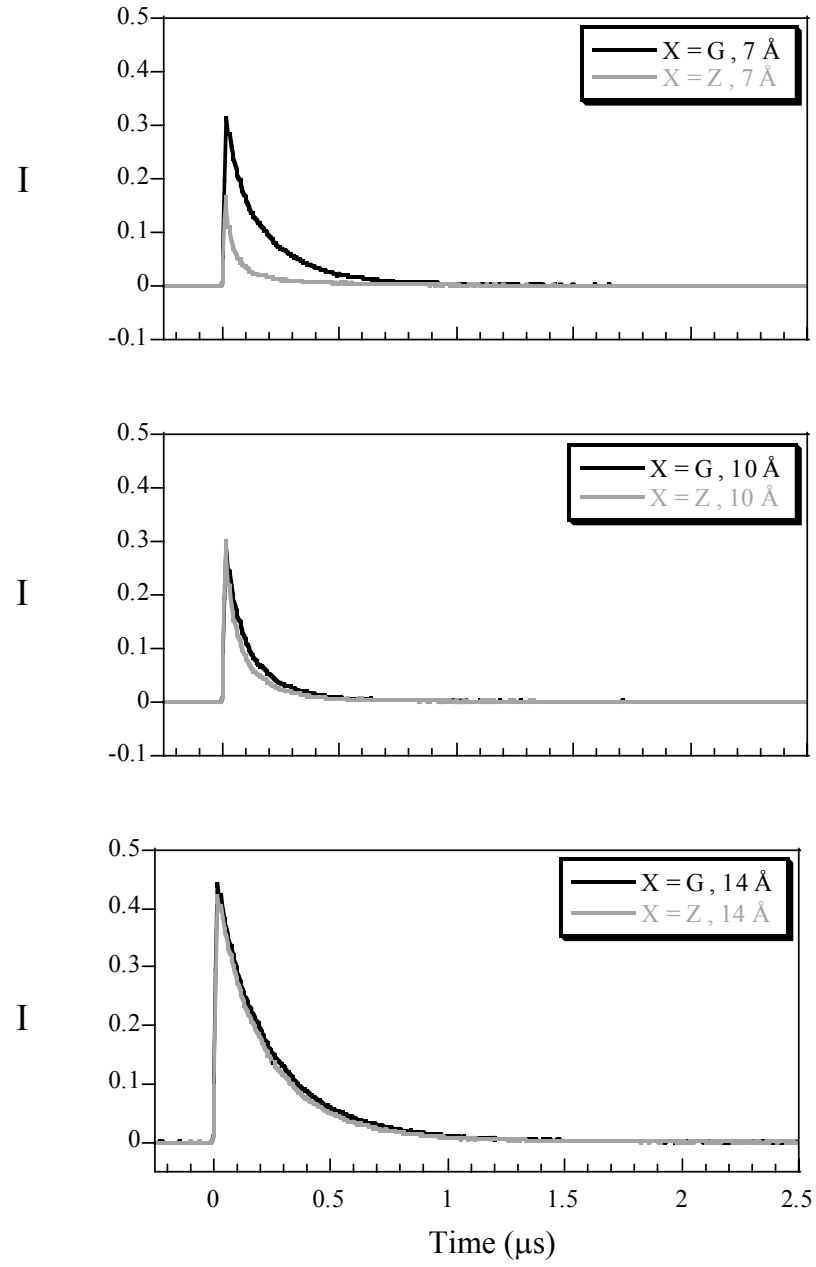

Figure 4.15 Time-resolved fluorescence of the G (black) and Z (gray) containing, $[Ru(phen)(phen')dppz]^{2+}$-modified DNA duplex series Δ3. Donor-acceptor distances are given in the Figure. λ_{exc}=480 nm, λ_{obs}=610 nm. 5 μM duplex in 5 mM NaPi, 50 mM NaCl, pH=7 buffer.

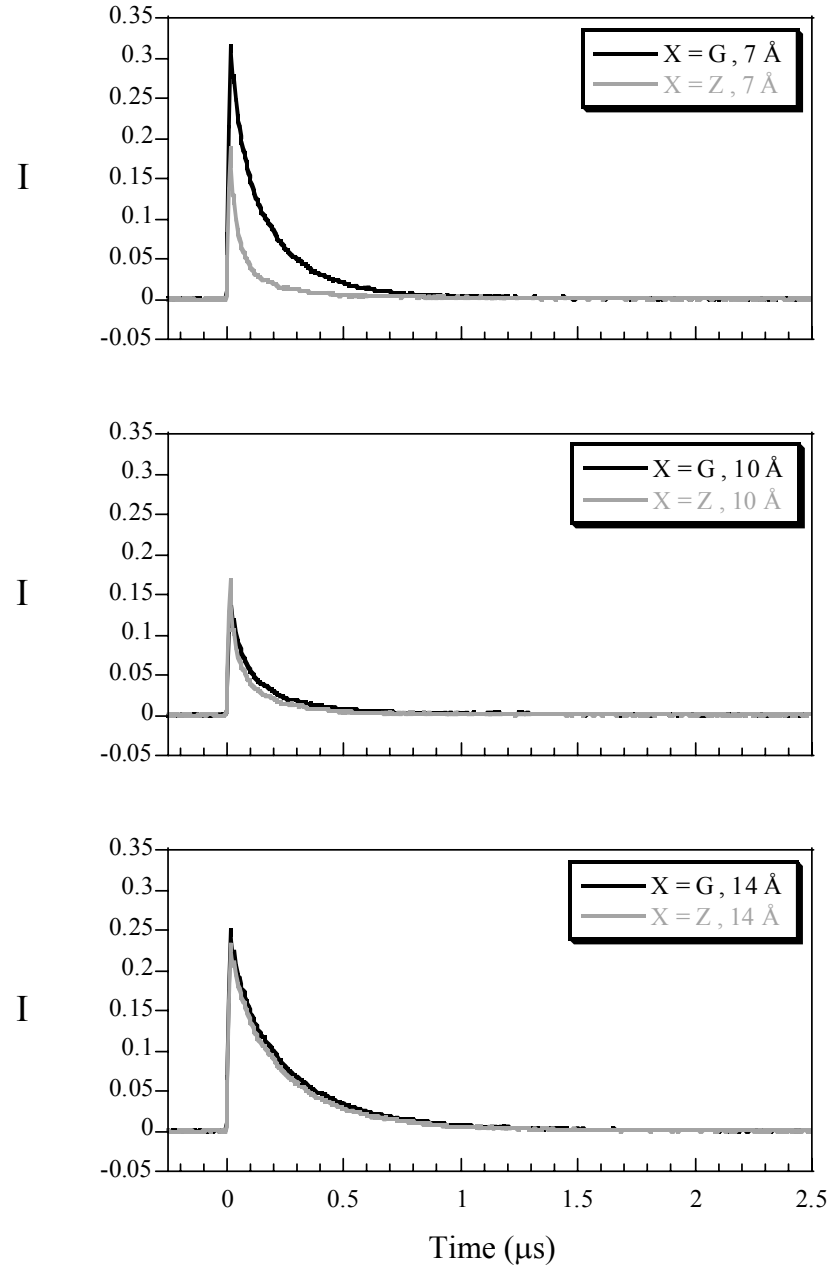

Figure 4.16 Time-resolved fluorescence of the G (black) and Z (gray) containing, $[Ru(phen)(phen')dppz]^{2+}$-modified DNA duplex series Δ4. Donor-acceptor distances are given in the Figure. λ_{exc}=480 nm, λ_{obs}=610 nm. 5 μM duplex in 5 mM NaPi, 50 mM NaCl, pH=7 buffer.

Sample[a]	Δ/Λ[b]	X=G[c] τ_1 (%τ_1)	X=G[d] τ_2 (%τ_2)	X=Z[e] τ_1 (%τ_1)	X=Z[f] τ_2 (%τ_2)
GXT7 1	Λ	250 (37%)	67 (63%)	220 (17%)	53 (83%)
GXT10 1	Λ	200 (27%)	54 (73%)	190 (26%)	52 (74%)
GXT14 4	Λ	340 (39%)	68 (61%)	340 (35%)	69 (65%)
GXT7 2	Λ	260 (20%)	64 (80%)	330 (6%)	45 (94%)
GXT10 2	Λ	310 (19%)	67 (81%)	300 (23%)	57 (77%)
GXT14 3	Λ	470 (71%)	81 (29%)	470 (70%)	85 (30%)
GXT7 3	Δ	220 (62%)	61 (38%)	310 (19%)	44 (81%)
GXT10 3	Δ	220 (27%)	77 (73%)	190 (29%)	54 (71%)
GXT14 1	Δ	300 (60%)	130 (40%)	280 (59%)	130 (41%)
GXT7 4	Δ	220 (56%)	68 (44%)	290 (19%)	49 (81%)
GXT10 4	Δ	310 (29%)	75 (71%)	240 (30%)	59 (70%)
GXT14 2	Δ	310 (65%)	110 (35%)	300 (64%)	100 (36%)

Table 4.3 Nanosecond lifetime data for Ru/G and Ru/Z modified DNA duplexes. (a) Sequence and HPLC peak number of the Ru-DNA conjugate. (b) Chirality about the metal center of the Ru-DNA conjugate. (c) and (d) Lifetimes (ns) and percentages of *Ru in Ru/G modified duplexes. (e) and (f) Lifetimes (ns) and percentages of *Ru in Ru/Z modified duplexes. Experimental conditions: 5 μM DNA duplex in 5 mM NaPi, 50 mM NaCl, pH=7.0 buffer with λ_{exc}=480 nm and λ_{obs}=610 nm. Data fit via the least-squares method to the equation $I(t) = c0+c1*\exp(-t/\tau_1)+c2*\exp(-t/\tau_2)$.

intercalator in the Λ-Ru/Z conjugates is not able to intercalate as well into the DNA base stack. The electronic coupling between Ru and Z is not as good in that case, and this manifests itself in a slower rate constant for charge transfer. Another explanation is that the observed rate constant is simply the time required for the ruthenium intercalator to become "well stacked" (and thus well coupled) in the DNA base stack. While a similar dynamical motion has been used to describe charge transfer in ethidium/7-deazaguanine duplexes, we cannot definitively say if that behavior is occurring in the Λ-Ru/Z DNA assemblies.[2] Nevertheless, the time-resolved data illustrate how subtle effects in DNA intercalation can drastically alter charge transfer mediated by the DNA base stack.

Transient Absorption. Can any other processes account for the ruthenium luminescence quenching by 7-deazaguanine? The redox potentials and lack of spectral overlap between Ru emission and Z absorption make this unlikely. However, we used transient absorption spectroscopy to identify an intermediate in the quenching reaction, thus definitely proving charge transfer is responsible for *Ru(II) luminescence quenching by 7-deazaguanine. Figure 4.17 (bottom graph) illustrates the differences in the transient absorption signals at 450 nm for the Δ3-Ru/Z and Δ3-Ru/G (7 Å) conjugates. The recovery times clearly match the excited-state fluorescence decays observed for the same duplexes (top graph). The transient signal in the Δ3-Ru/Z (7 Å) duplex actually rises above zero. This signal decays within 1 microsecond, and no long-lived transients are observed under the chosen experimental conditions.

In order to characterize the spectrum of the Ru/Z transient, measurements were taken over a large range of wavelengths. Figure 4.18 illustrates the transient spectrum from 350–520 nm for the Δ3-Ru/Z (7 Å) assembly. Above 520 nm, residual fluorescence overloads the photomultiplier tube and the signals are not indicative of the true transient spectrum. As seen by comparing this spectrum to the *Ru-Ru^{2+} spectrum shown in Figure 4.19, the observed species is definitely not assigned as ruthenium(II) excited state.

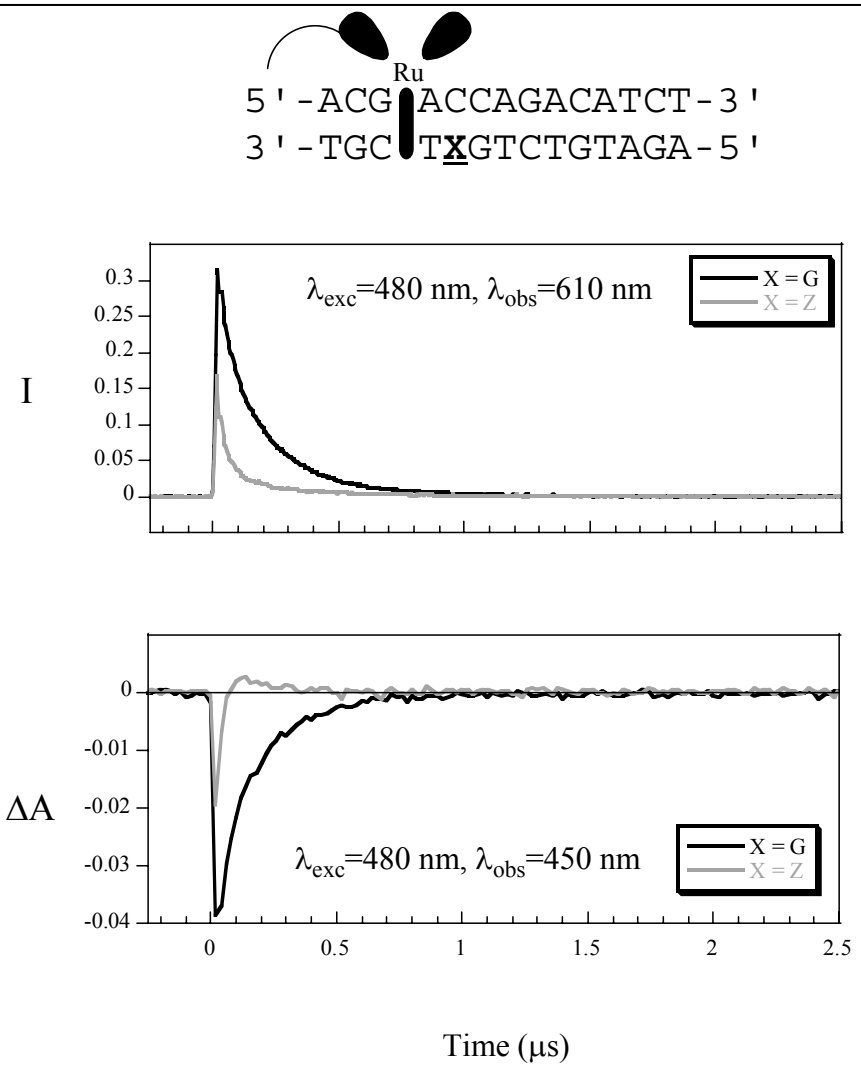

Figure 4.17 Time-resolved fluorescence (top) and transient absorption (bottom) of the Δ3 diastereomer of the G (black) and Z (gray) containing, $[Ru(phen)(phen')dppz]^{2+}$-modified DNA duplex shown in the Figure. Ru-G and Ru-Z distances are ca. 7 Å. 5 μM duplex in 5 mM NaPi, 50 mM NaCl, pH=7 buffer.

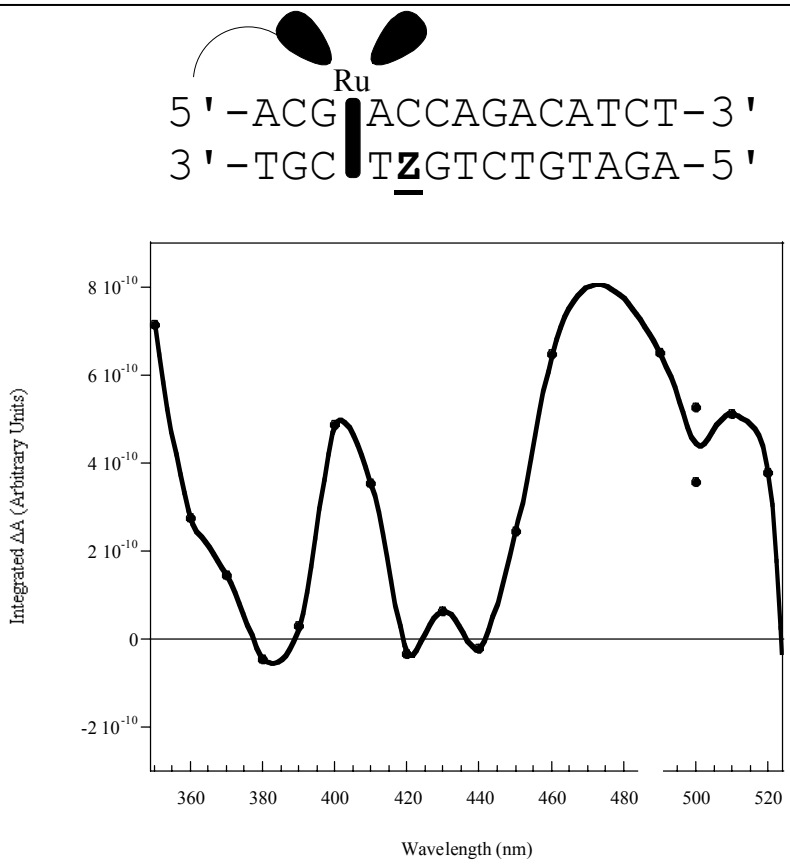

Figure 4.18 Transient absorption spectrum of the Δ3 diastereomer of the $[Ru(phen)(phen')dppz]^{2+}$-7-deazaguanine DNA conjugate shown in the Figure. Points obtained by integrating the area under the curve at each specific wavelength. 5 μM DNA duplex in 5 mM NaPi, 50 mM NaCl, pH=7 buffer with λ_{exc}=480 nm.

It is unclear if any of the spectral features correspond to the 7-deazaguanine radical, because the spectrum of the 7-deazaguanine radical is unknown. It is likely very similar to that of the guanine radical in DNA, which means that its spectroscopic signature would be weak and difficult to observe.[26] The spectrum does, however, match up very closely with the Ru(I) spectrum generated by the reaction of *Ru(II) with the electron transfer quencher triethanolamine in acetonitrile (middle of Figure 4.19). This provides definitive proof that quenching of ruthenium(II) luminescence in DNA by 7-deazaguanine generates ruthenium(I) and thus proceeds via a charge transfer mechanism.

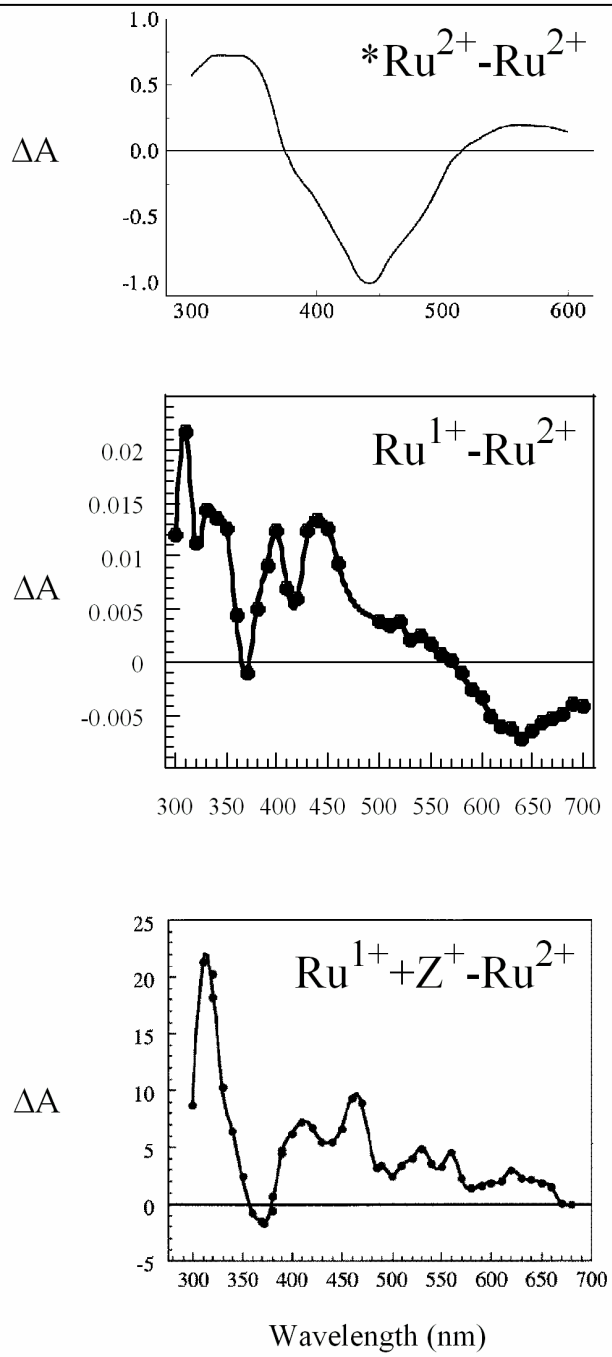

Figure 4.19 Transient absorption spectra for a variety of [Ru(phen)$_2$dppz] species. Top – Excited-state Ru(II) bound to DNA; Middle – Ru(I) generated by reaction of *Ru(II) with the reductive quencher triethanolamine; Bottom – Ru(I) plus 7-deazaguanine radical generated by exciting Ru(II) bound to a short piece of DNA containing multiple 7-deazaguanine bases. In all cases, λ_{exc}=480 nm.

The spectroscopic results obtained for Ru/Z assemblies reinforce the notion that stacking of the reactants within DNA plays a huge role in determining the efficiency and rate of DNA-mediated charge transfer. The behavior observed in Ru/Z assemblies, while still indicative of efficient charge transfer through the DNA double helix, was different than that observed in ethidium/Z and 2-aminopurine/Z systems (Table 4.4). Comparison of the results for the various systems leads to the conclusion that ethidium is able to best maintain stacking and coupling over a range of donor-acceptor distances. Rates of intrastrand charge transfer between Ap and Z fall off slightly with distance, as the stacking of the Ap is somewhat limited to one strand of the DNA double helix. While the Δ-Ru/Z charge transfer rates were unable to be resolved, they are faster than their Λ-Ru/Z counterparts in which the intercalator is more poorly stacked within the DNA.

DNA Assembly	D-A Distance	Charge Transfer Decay Time(s)
Ethidium/7-deazaguanine	10–17 Å	5 ps, 75 ps
2-Aminopurine/7-deazaguanine	3–14 Å	4 ps – 200 ps
Δ-Ruthenium/7-deazaguanine	7–14 Å	< 10 ns
Λ-Ruthenium/7-deazagunine	7–14 Å	ca. 100 ns

Table 4.4 Comparison of the DNA-mediated charge transfer behavior between 7-deazaguanine and a variety of photooxidants.

It is clear that subtle differences in the interaction of the reactants with the DNA base stack result in substantial differences of the observed charge transfer rates. While it would be convenient if charge transfer through DNA could be described by a simple set of parameters, the data in the last three chapters shows this is not reasonable for a system as complex as DNA in solution. Any future studies examining charge transfer through the double helix must take this into account.

4.4 Conclusions

The use of a classic dppz-based ruthenium(II) intercalator tethered to DNA has allowed us to further study the spectroscopic nuances of DNA-mediated charge transfer. Quenching of ruthenium(II) excited-state luminescence by 7-deazaguanine over distances of 7–14 Å through the DNA base stack was examined. The efficiency of the reaction was found to be on par with similar studies utilizing an intercalator and 7-deazaguanine as the donor-acceptor pair. The shallow distance dependence was also dependent upon the chirality about the metal center of the intercalator, indicating binding to DNA plays an important role in determining how charge transfer behaves. Time-resolved fluorescence revealed the process takes place on the nanosecond timescale, slightly slower than ultrafast charge transfer observed between ethidium and 7-deazaguanine. The unique spectroscopic properties of the ruthenium intercalator allowed the identification of a charge transfer intermediate, thus confirming that electron transfer is the mechanism of ruthenium luminescence quenching. These results once again emphasize the importance of stacking and electronic coupling to DNA-mediated charge transfer.

4.5 References

1. (a) Kelley, S. O.; Barton, J. K. *Chem. Biol.* **1998**, *5*, 413. (b) Steenken, S.; Jovanovic, S. V. *J. Am. Chem. Soc.* **1997**, *119*, 617.

2. Wan, C.; Fiebig, T.; Kelley, S. O.; Treadway, C. R.; Barton, J. K.; Zewail, A. H. *Proc. Natl. Acad. Sci. U.S.A.* **1999**, *96*, 6014.

3. Kelley, S. O.; Barton, J. K. *Science* **1999**, *283*, 375.

4. Wan, C.; Fiebig, T.; Schiemann, O.; Barton, J. K.; Zewail, A. H. *Proc. Natl. Acad. Sci. U.S.A.* **2000**, *97*, 14052.

5. Friedman, A. E.; Chambron, J.-C.; Sauvage, J.-P.; Turro, N. J.; Barton, J. K. *J. Am. Chem. Soc.* **1990**, *112*, 4960.

6. Jenkins, Y.; Friedman, A. E.; Turro, N. J.; Barton, J. K. *Biochemistry* **1992**, *32*, 10809.

7. Turro, C.; Bossman, S. H.; Jenkins, Y.; Barton, J. K.; Turro, N. J. *J. Am. Chem. Soc.* **1995**, *117*, 9026.

8. Olson, E. J. C.; Hu, D.; Hormann, A.; Jonkman, A. M.; Arkin, M. R.; Stemp, E. D. A.; Barton, J. K.; Barbara, P. F. *J. Am. Chem. Soc.* **1997**, *119*, 11458.

9. Arkin, M. R.; Stemp, E. D. A.; Holmlin, R. E.; Barton, J. K.; Hormann, A.; Olson, E. J. C.; Barbara, P. F. *Science* **1996**, *273*, 475.

10. Stemp, E. D. A.; Holmlin, R. E.; Barton, J. K. *Inorg. Chim. Acta* **2000**, *297*, 88.

11. Stemp, E. D. A.; Arkin, M. R.; Barton, J. K. *J. Am. Chem. Soc.* **1995**, *117*, 2375.

12. Delaney, S.; Pascaly, M.; Bhattacharya, P. K.; Han, K.; Barton, J. K. *Inorg. Chem*. **2002**, *41*, 1966.

13. Dickeson, J. E.; Summers, L. A. *Aust. J. Chem.* **1970**, *23*, 1023.

14. Waterland, M. R.; Gordon, K C.; McGarvey, J. M; Jayaweera, P. M. *J. Chem. Soc., Dalton Trans.* **1998**, 609.

15. Sullivan, B. P.; Salmon, D. J.; Meyer, T. J. *Inorg. Chem.* **1978**, *17*, 3334.

16. Amouyal, E.; Homsi, A.; Chambron, J.-C.; Sauvage, J.-P. *J. Chem. Soc., Dalton Trans.* **1990**, 1841.

17. Anderson, P. A.; Deacon, G. B.; Haarmann, K. H.; Keene, F. R.; Meyer, T. J.; Reitsma, D. A.; Skelton, B. W.; Strouse, G. F.; Thomas, N. C.; Treadway, J. A.; White, A. H. *Inorg. Chem*. **1995**, *34*, 6145.

18. Holmlin, R. E.; Dandliker, P. J.; Barton, J. K. *Bioconj. Chem.* **1999**, *10*, 1122.

19. Cantor, C. R.; Warshaw, M. M.; Shapiro, H. *Biopolymers* **1970**, *9*, 1059.

20. Warshaw, M. M.; Tinoco, I. *J. Mol. Bio.* **1966**, *1*, 29.

21. Yoshikawa, Y.; Yamasaki, K. *Coord. Chem. Rev.* **1979**, *28*, 205.

22. Lincoln, P.; Tuite, E.; Nordén, B. *J. Am. Chem. Soc.* **1997**, *119*, 1454.

23. Franklin, S. J.; Treadway, C. R.; Barton, J. K. *Inorg. Chem.* **1998**, *37*, 5198.

24. Barton, J. K. *Science* **1986**, *233*, 727.

25. Kumar, C. V.; Barton, J. K.; Turro, N. J. *J. Am. Chem. Soc.* **1985**, *107*, 5518.

26. Stemp, E. D. A.; Arkin, M. R.; Barton, J. K. *J. Am. Chem. Soc.* **1997**, *119*, 2921.